Inverse Polarization Raytracing: Estimating Surface Shapes of Transparent Objects

Daisuke Miyazaki Katsushi Ikeuchi

Institute of Industrial Science, The University of Tokyo, JAPAN
http://www.cvl.iis.u-tokyo.ac.jp/

Abstract

We propose a novel method for estimating the surface shapes of transparent objects by analyzing the polarization state of the light. Existing methods do not fully consider the reflection, refraction, and transmission of the light occurring inside a transparent object. We employ a polarization raytracing method to compute both the path of the light and its polarization state. Our proposed iterative computation method estimates the surface shape of the transparent object by minimizing the difference between the polarization data rendered by the polarization raytracing method and the polarization data obtained from a real object.

1. Introduction

In the field of computer vision, few methods have been proposed for estimating the shape of transparent objects, because of the difficulty of dealing with mutual reflection, which is the phenomenon that the light not only reflects at the surface of the transparent object but also transmits into the object and causes multiple reflections and transmissions inside it. In this paper, we use the term “interreflection” for such internal reflection. Raytracer simulates the interreflection, and renders the 2D image from 3D shape:

$$\mathsf{Image} = \mathsf{Raytracer}(\mathsf{Shape}) \quad . \tag{1}$$

If an inverse function of raytracing were to exist, the 3D shape could be obtained straightforwardly from 2D data; however, there is no closed-form solution for the inverse problem of raytracing. This paper presents a novel method for estimating the surface shape of transparent objects by numerically solving the inverse problem of raytracing and, at the same time, by analyzing the polarization of transparent objects.

An example for applying the proposed method is shown in Figure 1. Figure 1(a) is the target object, and Figure 1(b) is the result of proposed method. Figure 1(c) is a rendered example of the raytracing method by using the estimated shape.

Polarization is a phenomenon in which the light oscillates in one direction. Recently, research to estimate the shape of the object by using polarization has increased [1–5]. Saito et al. [6] and Miyazaki et al. [7,8] estimated the surface shape of transparent objects by means of polarization analysis. Unfortunately, because these methods do not consider interreflection, they do not provide sufficient accuracy for estimating the shape of transparent objects. Other methods that estimate the 3D shape of transparent objects without using polarization have been proposed. Murase [9] estimated the shape of a water surface by analyzing the undulation of the water surface. Hata et al. [10] estimated the surface shape of transparent objects by analyzing the deformation of the light projected onto the transparent objects. Ohara et al. [11] estimated the depth of the edge of a transparent object by using shape-from-focus. Ben-Ezra and Nayar [12] estimated the parameterized surface shape of transparent objects by using structure-from-motion. Kutulakos [13] estimated both the depth and the surface normal of transparent objects by multiple viewpoints and multiple light sources. These methods, however, do not estimate arbitrary shapes of transparent objects.

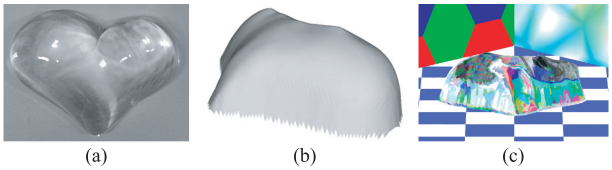

Figure 1: Result for heart-shaped glass: (a) Target object, (b) result of proposed method, (c) raytracing image.

There are other works that deal with transparent objects by using methods such as environment matting [14–19] and reflection separation [20–23]; however, they do not provide enough information about the shapes of the transparent objects.

We simulate the interreflection of transparent objects by using a method called polarization raytracing, and we use this method to estimate the surface shapes of transparent objects with arbitrary shapes. In this paper, a forward-facing surface of the transparent object is called a front surface, and an object surface facing away from the camera is called a back surface. Our proposed method estimates the shape of the front surface by using polarization raytracing when the refractive index, the shape of the back surface, and the illumination distribution are given.

The rest of the paper is organized as follows. In Section 2, we describe the theoretical background of the polarization raytracing method. In Section 3, we explain our estimation method, which solves the inverse problem of polarization raytracing method. Our measurement results are shown in Section 4, and our conclusions are presented in Section 5.

2. Polarization Raytracing

The theoretical details of the principle of polarization, which appears in this section, are presented in the literature [24, 25].

2.1. Conventional Raytracing

A conventional raytracing method renders a 2D image from 3D geometrical shape data of transparent objects or other kind of objects. The algorithm of the conventional raytracing method can be divided into two parts. The first part is the calculation of the propagation of the ray. The second part is the calculation of the intensity of the light.

Figure 2 describes the light reflected and transmitted between material 1 and material 2. Materials 1 and 2 may be, respectively, the air and the transparent object, and vice versa. Incidence angle, reflection angle, and transmission angle are defined in Figure 2. We assume that the surface of transparent objects is optically smooth; thus, the incidence angle is equal to the reflection angle. The transmission angle is related to the incidence angle as the following Snell's law:

$$\sin\theta = n\sin\theta' \quad , \tag{2}$$

where θ is the incidence angle, θ' is the transmission angle, and n is the ratio of the refractive index of material 2 to that of material 1. In this paper, we assume that the refractive index of one object is a scalar value which is, at the same time, constant throughout any part of the object. The plane of incidence (POI) is a plane that includes the surface normal direction, the incident light direction, the reflected light direction, and the transmitted light direction.

The intensity ratio of reflected light to incident light is called intensity reflectivity R, and the intensity ratio of transmitted light to incident light is called intensity transmissivity T. Subscripts $||$ and $\perp$ represent the components parallel and perpendicular to POI, respectively. Thus, parallel and perpendicular components of intensity reflectivity are represented as $R_{||}$ and $R_\perp$, respectively, while those of intensity transmissivity are represented as $T_{||}$ and $T_\perp$, respectively. These values are defined as follows:

$$R_{||} = \frac{\tan^2(\theta-\theta')}{\tan^2(\theta+\theta')} \tag{3}$$

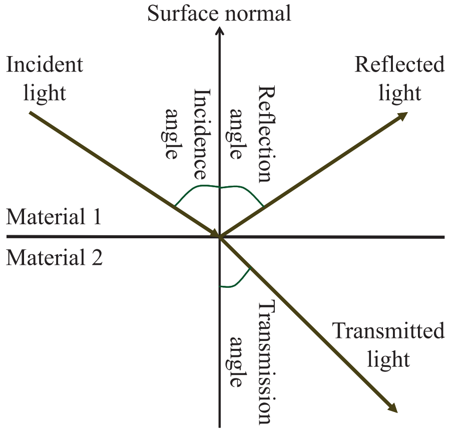

Figure 2: Reflection, refraction, and transmission.

$$R_\perp = \frac{\sin^2(\theta-\theta')}{\sin^2(\theta+\theta')} \tag{4}$$

$$T_{||} = \frac{\sin 2\theta \sin 2\theta'}{\sin^2(\theta+\theta')\cos^2(\theta-\theta')} \tag{5}$$

$$T_\perp = \frac{\sin 2\theta \sin 2\theta'}{\sin^2(\theta+\theta')} \quad . \tag{6}$$

If an incidence angle is larger than the critical angle, then the light does not transmit and totally reflects. This phenomenon is called total reflection and occurs when the incidence light is inside the object (namely, when material 1 is the object and material 2 is the air). Critical angle θ_C is defined as follows:

$$\sin\theta_c = n \quad . \tag{7}$$

For the total reflection, we must use $R_{||} = R_\perp = 1$ and $T_{||} = T_\perp = 0$.

The conventional raytracing method calculates the propagation of the ray by using the Snell's law (Equation (2)), and calculates the intensity of the light by using the total intensity reflectivity R and the total intensity transmissivity T, which are defined as follows:

$$R = \frac{R_{||}+R_\perp}{2} \ , \quad T = \frac{T_{||}+T_\perp}{2} \ . \tag{8}$$

2.2. Mueller Calculus

In this paper, we call the raytracing method that considers the polarization effect the polarization raytracing method. The algorithm of the polarization raytracing method can be divided into two parts. For the first part, the calculation of the propagation of the ray, we employ the same algorithm used in the conventional raytracing method. For the second part, the calculation of the polarization state of the light, there are three famous methods: Mueller calculus, Jones calculus, and the method that uses the coherence matrix. In this paper, we employ Mueller calculus because of its simplicity of description, along with its ease of understanding and implementation. These three methods have

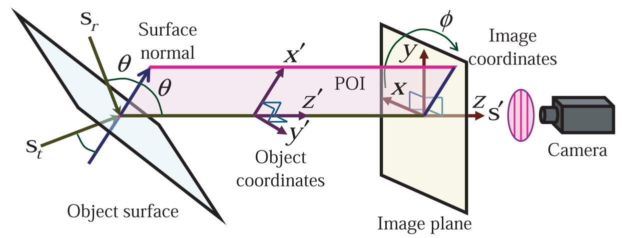

Figure 3: Reflected and transmitted light observed by the camera.

almost identical functions; thus, all discussions presented in this paper are also applicable to other calculi. Some researchers [26–32] also implemented and improved the polarization raytracing or improved these three methods, and also, there is some commercial software [33–35] that uses polarization raytracing.

In Mueller calculus, the polarization state of the light is represented as Stokes vector $\mathbf{s} = (s_0, s_1, s_2, s_3)^T$. The Stokes vector is a 4D vector. Its first component s_0 represents the intensity of the light; its second component s_1 represents the horizontal power of the linear polarization; its third component s_2 represents the $+45°$-oblique power of the linear polarization; and its fourth component s_3 represents the power of the right circular polarization. The Mueller matrix $\mathbf{M}$, which is a 4×4 matrix, represents how the object changes the polarization state of the light. The operation of Mueller calculus is a linear operation.

2.3. Mueller Matrices

In this section, we present an example of calculation using Mueller calculus.

Suppose the geometrical setup when the reflected and transmitted light is observed from the camera is as described in Figure 3. In this figure, there are two kinds of coordinates sytems: $x'y'z'$ coordinates and xyz coordinates. Here, the z' axis and the z axis are the same. x' is included in the POI and is facing to the same side as the surface normal is facing. The angle between x' axis and x axis is called the POI angle ϕ in xyz coordinates.

In the case presented in Figure 3, observed light is a composition of reflected light and transmitted light. The Stokes vector $\mathbf{s}'$ of the observed light is calculated as follows:

$$\begin{aligned}\mathbf{s}' &= \mathbf{C}(\phi)\mathbf{D}(\delta;n)\mathbf{R}(\theta;n)\mathbf{C}(-\phi)\mathbf{s}_r \\ &+ \mathbf{C}(\phi)\mathbf{T}(\theta;n)\mathbf{C}(-\phi)\mathbf{s}_t \quad . \qquad (9)\end{aligned}$$

Stokes vectors of the incident light are represented as $\mathbf{s}_r$ and $\mathbf{s}_t$, and where $\mathbf{s}_r$ and $\mathbf{s}_t$ represent the lights that are set in the origin of the reflection and transmission, respectively. $\mathbf{C}$ is the rotation Mueller matrix and is given by:

$$\mathbf{C}(\phi) = \begin{pmatrix} 1 & 0 & 0 & 0 \\ 0 & \cos 2\phi & -\sin 2\phi & 0 \\ 0 & \sin 2\phi & \cos 2\phi & 0 \\ 0 & 0 & 0 & 1 \end{pmatrix} \quad . \qquad (10)$$

$\mathbf{R}$ and $\mathbf{T}$ are the reflection Mueller matrix and the transmission Mueller matrix, respectively, which are represented as follows:

$$\mathbf{R} = \begin{pmatrix} (R_{||}+R_\perp)/2 & (R_{||}-R_\perp)/2 & 0 & 0 \\ (R_{||}-R_\perp)/2 & (R_{||}+R_\perp)/2 & 0 & 0 \\ 0 & 0 & \sqrt{R_{||}R_\perp} & 0 \\ 0 & 0 & 0 & \sqrt{R_{||}R_\perp} \end{pmatrix} \qquad (11)$$

$$\mathbf{T} = \begin{pmatrix} (T_{||}+T_\perp)/2 & (T_{||}-T_\perp)/2 & 0 & 0 \\ (T_{||}-T_\perp)/2 & (T_{||}+T_\perp)/2 & 0 & 0 \\ 0 & 0 & \sqrt{T_{||}T_\perp} & 0 \\ 0 & 0 & 0 & \sqrt{T_{||}T_\perp} \end{pmatrix} \quad . \qquad (12)$$

However, if the total reflection occurs, that is, if the incidence angle θ is larger than critical angle θ_C, then $\mathbf{R}$ and $\mathbf{T}$ are set to be identity matrix and zero matrix, respectively. $\mathbf{D}$ is the retardation Mueller matrix and is given as:

$$\mathbf{D}(\delta) = \begin{pmatrix} 1 & 0 & 0 & 0 \\ 0 & 1 & 0 & 0 \\ 0 & 0 & \cos\delta & \sin\delta \\ 0 & 0 & -\sin\delta & \cos\delta \end{pmatrix} \quad , \qquad (13)$$

where δ is the amount of the phase shift (*or* retardation). The phase of the reflected light shifts when the total reflection occurs. Thus, for the total reflection, δ in the following equation is used.

$$\tan\frac{\delta}{2} = \frac{\cos\theta\sqrt{\sin^2\theta - n^2}}{\sin^2\theta} \quad . \qquad (14)$$

The phase of the reflected light inverts when the incidence angle is smaller than the Brewster angle θ_B, which is defined as follows:

$$\tan\theta_B = n \quad . \qquad (15)$$

Thus, the value of δ is set as follows:

$$\delta = \begin{cases} \text{Eq.(14)} & \theta \geq \theta_C \\ 180° & \theta \leq \theta_B \\ 0° & \text{otherwise} \end{cases} \quad . \qquad (16)$$

2.4. Degree of Polarization

The polarization state of the light is calculated by observing the object with a monochrome camera, which has a linear polarizer in the front. For a certain pixel, we denote the maximum intensity observed by rotating the polarizer as $I_{\max}$ and the minimum as $I_{\min}$. The angle of the polarizer when the minimum intensity $I_{\min}$ is observed is called the phase angle ψ. This angle is defined as the angle from $+x$ axis to $+y$ axis in xyz coordinates (Figure 3).

Because the linear polarizer is used in this research, the fourth parameter s_3 of the Stokes vector cannot be determined. The relationship between the Stokes vector $(s_0, s_1, s_2)^T$ and $I_{\max}$, $I_{\min}$, ψ is:

$$\begin{pmatrix} s_0 \\ s_1 \\ s_2 \end{pmatrix} = \begin{pmatrix} 1 & 0 & 0 \\ 0 & \cos 2\psi & -\sin 2\psi \\ 0 & \sin 2\psi & \cos 2\psi \end{pmatrix} \begin{pmatrix} I_{\max} + I_{\min} \\ I_{\max} - I_{\min} \\ 0 \end{pmatrix} . \qquad (17)$$

The degree of polarization (DOP) represents how much the light is polarized and is defined as follows:

$$\hat{\rho} = \frac{\sqrt{s_1^2 + s_2^2 + s_3^2}}{s_0} \quad . \tag{18}$$

However, linear polarizer can only calculate the following degenerated DOP:

$$\rho = \frac{I_{\max} - I_{\min}}{I_{\max} + I_{\min}} = \frac{\sqrt{s_1^2 + s_2^2}}{s_0} \quad . \tag{19}$$

For the remainder of this paper, we refer to the ratio calculated by Equation (19) as DOP.

2.5. Illumination Distribution

In this paper, we assume that all light sources are unpolarized. We also assume that the front surface of the object is uniformly illuminated with the same intensity in every direction, and that the back surface of the object is also uniformly illuminated with the same intensity in every direction but with a different intensity from the intensity that illuminates the front surface.

3. Inverse Polarization Raytracing

In this section, we introduce our method for estimating the front surface shape of a transparent object using the DOP and the phase angle as inputs under the assumption that the refractive index, the shape of the back surface, and the illumination distribution are given. Details of numerical algorithms are shown in the literature [36].

We denote the input polarization data as I_E. Polarization data are represented as an image (2-dimensionally distributed data) where the DOP and phase angle are set for each pixel. The polarization raytracing explained in Section 2 can render the polarization data from the shape of the transparent object by tracing the light ray and by Mueller calculus. We denote this rendered polarization image as I_R. The shape of transparent objects is represented as the height H, set for each pixel. Heights partially differentiated by x and y are called gradients, and are represented as p and q, respectively:

$$p = H_x = \frac{\partial H}{\partial x}, \quad q = H_y = \frac{\partial H}{\partial y} \quad . \tag{20}$$

Surface normal $\mathbf{n} = (-p, -q, 1)^T$ is represented by these gradients.

The rendered polarization image I_R depends upon height and surface normal, so it can be represented as $I_R(H, p, q)$. Our problem is finding the best values to reconstruct a surface H that satisfies the following equation:

$$I_E = I_R(H, p, q) \quad . \tag{21}$$

We call this equation the "polarization raytracing equation" from the analogy of "image irradiance equation" used in the shape-from-shading problem.

A straightforward definition of the cost function, which we want to minimize, can be as follows:

$$\iint E_1(x, y) dx dy \quad , \tag{22}$$

where,

$$E_1 = (I_E - I_R(H, p, q))^2 \quad . \tag{23}$$

We will sometimes omit the variables (x, y) in the subsequent discussions for the simplicity of descriptions. I_R depends upon p, q, and H, while p, q, and H depend upon each other with Equation (20). Thus, the cost function must be modified as follows:

$$\iint (\lambda E_1 + E_2)\, dx dy \quad , \tag{24}$$

where,

$$E_2 = (H_x - p)^2 + (H_y - q)^2 \quad . \tag{25}$$

λ is a Lagrange undetermined multiplier.

Euler equations that minimize Equation (24) are derived as follows:

$$p = H_x - \frac{\lambda}{2} \frac{\partial E_1}{\partial p} \tag{26}$$

$$q = H_y - \frac{\lambda}{2} \frac{\partial E_1}{\partial q} \tag{27}$$

$$H = \bar{H} - \frac{1}{4}(p_x + q_y) - \frac{\lambda}{8} \frac{\partial E_1}{\partial H} \quad , \tag{28}$$

where $\bar{H}$ is a 4-neighbor average of H.

Each of the above equations can be decomposed into two steps:

$$p^{(k)} = H_x^{(k)} \tag{29}$$

$$p^{(k+1)} = p^{(k)} - \lambda_1^{(k+1)} \frac{\partial E_1^{(k)}}{\partial p} \tag{30}$$

$$q^{(k)} = H_y^{(k)} \tag{31}$$

$$q^{(k+1)} = q^{(k)} - \lambda_2^{(k+1)} \frac{\partial E_1^{(k)}}{\partial q} \tag{32}$$

$$H^{(k+1)} = \bar{H}^{(k)} - \frac{1}{4}\left(p_x^{(k+1)} + q_y^{(k+1)}\right) \tag{33}$$

$$H^{()} = H^{()} - \lambda_3^{()} \frac{\partial E_1^{()}}{\partial H} \quad . \tag{34}$$

Here, λ_1, λ_2, and λ_3 are scalar values that are determined for each pixel and for each iteration step. Superscript (k) represents the iteration number. We do not write down the iteration number for Equation (34) because we do not use this equation due to the following reasons. One reason is that the cost function E_1 depends upon the change of surface normal rather than on the change of height. Another reason is that the cost function E_1 smoothly changes when the surface normal changes, but it does not smoothly change when the height changes. This fact was empirically proved in the preliminary experiments.

The algorithm goes as follows. First, we set initial values of the shape H for each point of the front surface. Next, p and q are calculated by Equations (29)(31). Then, we solve Equations (30)(32). λ_1 and λ_2 should be optimal values; thus, we use Brent's method to determine λ_1 and λ_2, which minimizes the cost function E_1. After computing p and q at every pixel, we solve Equation (33) by the relaxation method [37,38] to determine the height H. We use the alternating-direction implicit method to solve the relaxation problem.

To conclude, the front surface shape of the transparent object is estimated by an iterative computation, where each step of iteration solves Equations (29)–(33), and the iteration stops when Equation (22) is minimized. There are two reasons why we use Equations (29)–(33) instead of Equations (26)–(28): (1) If we solve Equations (26)–(28) simultaneously by setting an arbitrary value λ, a parameter tuning problem will occur where λ must be set to an optimal value in order to stably solve these equations; (2) We can apply adequate numerical algorithms for each of Equations (29)–(33).

4. Measurement Result

4.1. Acquisition System

For obtaining polarization data, we developed an acquisition system, which we named "Cocoon" (Figure 4). The target object is set inside the center of the plastic sphere whose diameter is 35cm. This plastic sphere is illuminated by 36 incandescent lamps. These 36 light sources are almost uniformly distributed spatially around the plastic sphere. The plastic sphere diffuses the light that comes from the light sources, and it behaves as a spherical light source, which illuminates the target object from every direction. Note that the measurement is possible for arbitrary illumination conditions though the intensity and the polarization state of the illumination distribution must be known. The target object is observed by monochrome camera from the top of the plastic sphere, which has a hole on the top. Linear polarizer is set in front of the camera. We put the target object on the black pipe to make the incoming light from the back surface uniform and unpolarized. The camera, object, and light sources are fixed. From four images taken by rotating the polarizer at $0°$, $45°$, $90°$, and $135°$, we calculate $I_{\max}$, $I_{\min}$, and ψ (Section 2.4).

4.2. Rendering Result

Before estimating the shape of the transparent object, we analyze the rendered image of forward polarization raytracing (Section 2). From the spherical part, we observe a transparent acrylic hemisphere, whose refractive index is 1.5 and diameter is 3cm. Obtained polarization image of the real object is shown in Figure 5(a). The figure represents the DOP, where DOP 0 and DOP 1 are represented as black and white, respectively.

The rendered polarization image of polarization raytracing is shown in Figure 5(b). The refractive index and the shape of the object are known. As for the illumination distribution, we have to obtain the ratio of the intensity of the light illuminating the front surface to that illuminating the back surface. Unfortunately, it is impossible to observe the light illuminating the back surface without moving the object out of the way. Therefore, we find the most appropriate value of the intensity of the back surface where the difference of the obtained DOP (Figure 5(a)) and the rendered DOP (Figure 5(b)) minimizes, by solving such minimization problem. Figure 5(b) is calculated by using the intensity obtained from such minimization.

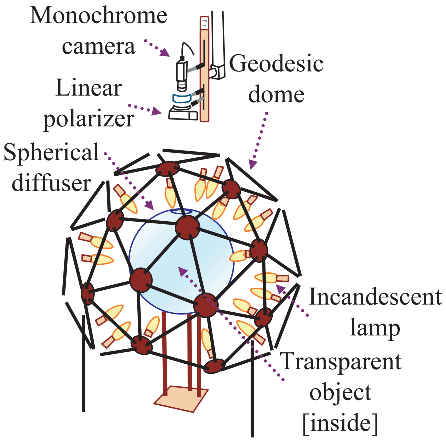

Figure 4: Acquisition System "Cocoon".

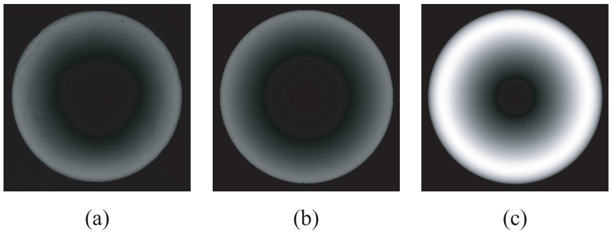

Figure 5: DOP image; (a) obtained from real object, (b) rendered by polarization raytracing, and (c) rendered by assuming that the internal interreflection does not occur.

For comparison, a rendered image with no interreflection is shown in Figure 5(c). This DOP image is rendered by assuming that the light reflected at the object's surface once is just observed and that the transmission does not occur. The root mean square (RMS) error between real data (Figure 5(a)) and DOP data of no interreflection (Figure 5(c)) was 0.48, while the RMS error between real data and polarization raytracing data (Figure 5(b)) was 0.055.

4.3. Simulation Result

Here, we will show the result of estimating the 2D shape of a simulated object for evaluating the robustness of our algorithm. This virtual transparent object is a concave shape whose refractive index is 1.5. The object is represented as a dotted line in Figure 6. We render the polarization data of

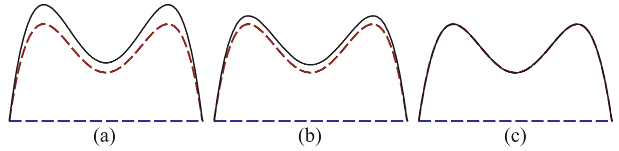

Figure 6: Simulation result of concave shape: (a) Initial state, (b)(c) result after 5, 20 loops, respectively.

the object observed from the upper position to the lower direction, and after that, we estimate the front surface shape of the concave object by using the rendered polarization data as input data. Illumination is distributed uniformly from every direction with the same intensity. The light is not illuminated at the bottom of the shape but is illuminated on the front surface. Illumination distribution, the back surface shape, and the refractive index are given.

The estimation result is illustrated in Figure 6. The dotted line is the true shape, and the solid line is the estimated shape. Figure 6(a) indicates the initial value, and Figure 6(b) and Figure 6(c) indicate the results after 5 and 20 loops of the proposed method. The shape, which is generated by scaling the true height by 1.2, is used as the initial state of the shape. The shape converged to the true shape at 20 loops. The average computation time was 14.8[sec] for 1 loop with 320 pixels by using Pentium4 3.4GHz. Here, the maximum number of tracings is 100 reflections or transmissions; however, if the energy of the light ray becomes less than a certain threshold, the tracing of the light ray is stopped.

4.4. Measurement Results of Real Object

4.4.1. Hemisphere

For the first measurement result, we observe an acrylic transparent hemisphere from the spherical part, which is also used in the rendering experiment (Section 4.2). We assume that the refractive index and the back surface shape are known. We use the same value for the intensity of the light source, which is obtained in Section 4.2. The value is obtained by observing the same object as Section 4.2, and we will provide a more objective result in the next section.

The estimation result is shown in Figure 7. Figure 7(a) represents the result of the previous method [6–8] and, at the same time, it represents the intial value. Figure 7(b) is the result after 10 loops of our method. The average computation time was 36[sec] for 1 loop with 7,854 pixels. Here, the maximum number of tracings is 10 reflections or transmissions.

More detailed evaluation is done in the 2D plane that is a cross section of the 3D object, which includes the center of the base circle and the line perpendicular to that circle. A light ray that is inside this plane does not go out, and a light ray that is outside this plane does not come in. The proposed algorithm estimates the front surface shape, a semicircle, by using the polarization data of the 2D plane as input data.

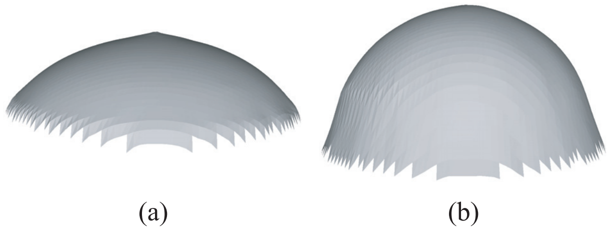

Figure 7: Estimation result of hemisphere: (a) Initial state (result of previous method), (b) result after 10 loops.

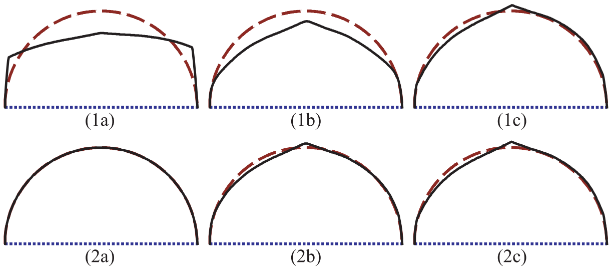

Figure 8: Estimation result: (1a) Initial state (result of previous method), (1b)(1c) results after 5 and 50 loops, (2a) initial state (true shape), (2b)(2c) results after 5 and 50 loops.

The result of applying the proposed method is given in Figure 8(1c) and Figure 8(2c). In Figure 8, the solid line represents the estimated shape, and the dotted line represents the true shape. For the estimated result shown in Figure 8(1c), the result of the previous method (Figure 8(1a)) is used for the initial state of the shape. For the estimated result shown in Figure 8(2c), the true shape, hemisphere (Figure 8(2a)), is used for the initial state of the shape. Figures 8(1b)(2b) and Figures 8(1c)(2c) are the result after 5 and 50 loops, respectively. The shapes converge to the same shape even if the initial shapes are different. The reason why there is a protruding noise at the top of the estimated shape might be the failure of considering the hole on top of the plastic sphere. Although we have assumed that the object is illuminated uniformly with the same intensity from all directions, we now believe that this assumption might not strictly hold for this hole. Therefore, considering such illumination distribution will be our future work.

The value of the cost function (Equation (22)) per each iteration is plotted in Figure 9. The vertical axis in Figure 9 represents the value of Equation (22), while the horizontal axis represents the iteration number. A diamond mark is the value of the result whose initial state is the result of the previous method (Figures 8(1a)(1b)(1c)). A square mark is the value of the result whose initial state is the true shape (Figures 8(2a)(2b)(2c)). The leftmost value is the value of the cost function of the initial state. Both the value and the shape did not change after around 8 loops. The average computation time was 5.9[sec] for 1 loop with 320 pixels.

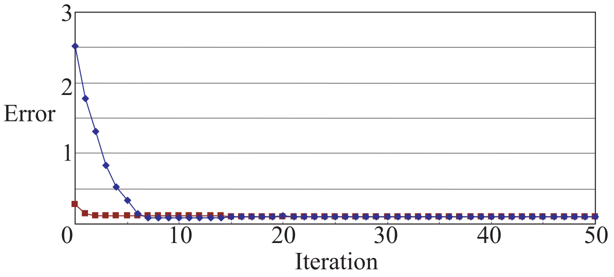

Figure 9: Error for each loop: (square) Result when true shape is initial value, (diamond) result when result of previous method is initial value.

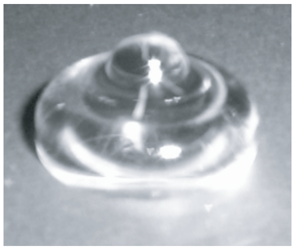

Figure 10: Bell-shaped transparent acrylic real object.

The RMS error between the estimated value and the true value is used to compare the accuracy between the proposed method and the previous method. The RMS error of the surface normal was 23.3° for previous method, 9.09° for our method when the initial state was the result of the previous method, and 8.86° for our method when the initial state was the true shape. The RMS error of the height was 2.70mm for the previous method, 0.672mm for our method when the initial state was the result of previous method, and 0.548mm for our method when the initial state was the true shape.

4.4.2. Bell-shaped Object

Finally, we observe the transparent object shown in Figure 10. This object is made of acrylic and is a body-of-revolution. Its refractive index is 1.5 and its diameter of the base is 24mm. The object is observed from the projected area of the object. The front surface is a curved surface and the back surface is a disk. The camera is set orthogonally to the disk. We assume that the refractive index and the back surface shape are known. We use the same value for the intensity of the light source that is obtained in Section 4.2. This paper only concentrates on proposing a method to estimate the shapes of transparent objects, and obtaining the correct illumination distribution will be a future work.

We estimate the shape of a cross-section of the object to analyze the precision of the proposed method. The cross-section includes the center of the base circle and the line perpendicular to that circle. Figure 11(c) illustrates the estimated shape of the object. The solid curve represents the obtained front height, and the dotted line represents the given back height. The initial value is set to be a semi-circle shown in Figure 11(a). The estimated shape after 5 and 20 loops is illustrated in Figure 11(b) and Figure 11(c), respectively. RMS of the height was 0.24mm, where the true shape was obtained from the silhouette extracted manually by a human operator from the photograph of the object taken from the side. The average computation time was 7.0[sec] for 1 loop with 320 pixels.

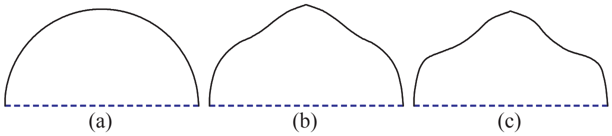

Figure 11: Estimation result: (a) Initial value, (b)(c) result after 5, 20 loops.

5. Conclusion

In this paper, we have proposed a novel method for estimating the surface shape of transparent objects by minimizing the difference between the input polarization data taken by observing the transparent object and the computed polarization data rendered by the polarization raytracing method.

We estimated the shape of transparent objects by an iterative computation. We used a uniform illumination in this paper; however, Hata et al. [10] estimated the shape of transparent objects by an iterative computation where the object was illuminated by structured light. Ben-Ezra and Nayar [12] estimated the shape of a transparent object observed from many viewpoints by an iterative computation. To improve the precision of measuring the surface shape of transparent objects, we should probably observe the target object from multiple viewpoints or under various types of illumination. In any case, the iterative computation is considered to be necessary. Our paper provides the technique for measuring the surface shape of transparent objects using iterative computation, and this technique might be used as the basis for further developments.

Most of the artificial transparent objects have a planar base that enables them to stand by themselves. Also, the material (refractive index) of the artificial transparent objects is known in many cases. Thus, the assumption we adopted in this paper, “back surface shape and refractive index are known,” is effective in many cases. However, not all objects meet these conditions; thus, we intend to develop a method that can measure the back surface shape and refractive index at the same time as well as the front surface shape.

Acknowledgments

This research was supported in part by the Ministry of Education, Culture, Sports, Science and Technology. Daisuke Miyazaki was supported by the Japan Society for the Promotion of Science. The authors thank Joan Knapp for proofreading and editing this manuscript. They also thank anonymous reviewers for their careful reviews of the paper.

References

[1] K. Koshikawa and Y. Shirai, "A model-based recognition of glossy objects using their polarimetrical properties," *Advanced Robotics*, Vol. 2, No. 2, pp. 137-147, 1987.

[2] L. B. Wolff and T. E. Boult, "Constraining object features using a polarization reflectance model," *IEEE Trans. Patt. Anal. Mach. Intell.*, Vol. 13, No. 7, pp. 635-657, 1991.

[3] S. Rahmann and N. Canterakis, "Reconstruction of specular surfaces using polarization imaging," *Proc. IEEE Conf. Computer Vision and Pattern Recognition*, pp. 149-155, 2001.

[4] O. Drbohlav and R. Šára, "Unambiguous determination of shape from photometric stereo with unknown light sources," *Proc. IEEE Int'l Conf. Computer Vision*, pp. I:581-586, 2001.

[5] D. Miyazaki, R. T. Tan, K. Hara, and K. Ikeuchi, "Polarization-based inverse rendering from a single view," *Proc. IEEE Int'l Conf. Computer Vision*, pp. 982-987, 2003.

[6] M. Saito, Y. Sato, K. Ikeuchi, and H. Kashiwagi, "Measurement of surface orientations of transparent objects by use of polarization in highlight," *J. Opt. Soc. Am. A*, Vol. 16, No. 9, pp. 2286-2293, 1999.

[7] D. Miyazaki, M. Saito, Y. Sato, and K. Ikeuchi, "Determining surface orientations of transparent objects based on polarization degrees in visible and infrared wavelengths," *J. Opt. Soc. Am. A*, Vol. 19, No. 4, pp. 687-694, 2002.

[8] D. Miyazaki, M. Kagesawa, and K. Ikeuchi, "Transparent surface modeling from a pair of polarization images," *IEEE Trans. Patt. Anal. Mach. Intell.*, Vol. 26, No. 1, pp. 73-82, 2004.

[9] H. Murase, "Surface shape reconstruction of a nonrigid transparent object using refraction and motion," *IEEE Trans. Patt. Anal. Mach. Intell.*, Vol. 14, No. 10, pp. 1045-1052, 1992.

[10] S. Hata, Y. Saitoh, S. Kumamura, and K. Kaida, "Shape extraction of transparent object using genetic algorithm," *Proc. Int'l Conf. Pattern Recognition*, pp. 684-688, 1996.

[11] K. Ohara, M. Mizukawa, K. Ohba, and K. Taki, "3D modeling of micro transparent object with integrated vision," *Proc. IEEE Conf. Multisensor Fusion and Integration for Intelligent Systems*, pp. 107-112, 2003.

[12] M. Ben-Ezra and S. K. Nayar, "What does motion reveal about transparency?," *Proc. IEEE Int'l Conf. Computer Vision*, pp. 1025-1032, 2003.

[13] K. N. Kutulakos, "Refractive and specular 3D shape by light-path triangulation," *Proc. Int'l Symposium on the CREST Digital Archiving Project*, pp. 86-93, 2005.

[14] D. E. Zongker, D. M. Warner, B. Curless, and D. H. Salesin, "Environmental matting and compositing," *Proc. SIGGRAPH*, pp. 205-214, 1999.

[15] Y. Chuang, D. E. Zongker, J. Hindorff, B. Curless, D. H. Salesin, and R. Szeliski, "Environment matting extensions: towards higher accuracy and real-time capture," *Proc. SIGGRAPH*, pp. 121-130, 2000.

[16] Z. S. Hakura and J. M. Snyder, "Realistic reflections and refractions on graphics hardware with hybrid rendering and layered environment maps," *Proc. Eurographics Workshop on Rendering*, pp. 289-300, 2001.

[17] W. Matusik, H. Pfister, R. Ziegler, A. Ngan, and L. McMillan, "Acquisition and rendering of transparent and refractive objects," *Proc. Eurographics Workshop on Rendering*, pp. 267-278, 2002.

[18] Y. Wexler, A. W. Fitzgibbon, and A. Zisserman, "Image-based environment matting," *Proc. Eurographics Workshop on Rendering*, pp. 279-290, 2002.

[19] P. Peers and P. Dutré, "Wavelet environment matting," *Proc. Eurographics Workshop on Rendering*, pp. 157-166, 2003.

[20] Y. Y. Schechner, J. Shamir, and N. Kiryati, "Polarization and statistical analysis of scenes containing a semireflector," *J. Opt. Soc. Am. A*, Vol. 17, No. 2, pp. 276-284, 2000.

[21] Y. Y. Schechner, N. Kiryati, and R. Basri, "Separation of transparent layers using focus," *Int'l J. Computer Vision*, Vol. 39, No. 1, pp. 25-39, 2000.

[22] R. Szeliski, S. Avidan, and P. Anandan, "Layer extraction from multiple images containing reflections and transparency," *Proc. IEEE Conf. Computer Vision and Pattern Recognition*, pp. 246-253, 2000.

[23] H. Farid and E. H. Adelson, "Separating reflections from images by use of independent component analysis," *J. Opt. Soc. Am. A*, Vol. 16, No. 9, pp. 2136-2145, 1999.

[24] M. Born and E. Wolf, *Principles of optics*, Pergamon Press, 1959.

[25] W. A. Shurcliff, *Polarized light: production and use*, Harvard University Press, 1962.

[26] R. A. Chipman, "Mechanics of polarizaiton ray tracing," *Optical Engineering*, Vol. 34, No. 6, pp. 1636-1645, 1995.

[27] L. B. Wolff and D. J. Kurlander, "Ray tracing with polarization parameters," *IEEE Computer Graphics and Applications*, Vol. 10, No. 6, pp. 44-55, 1990.

[28] C. Gu and P. Yeh, "Extended Jones matrix method. II," *J. Opt. Soc. Am. A*, Vol. 10, No. 5, pp. 966-973, 1993.

[29] J. S. Gondek, G. W. Meyer, and J. G. Newman, "Wavelength dependent reflectance functions," *Proc. SIGGRAPH*, pp. 213-220, 1994.

[30] D. C. Tannenbaum, P. Tannenbaum, and M. J. Wozny, "Polarization and birefringency considerations in rendering," *Proc. SIGGRAPH*, pp. 221-222, 1994.

[31] A. Wilkie, R. F. Tobler, and W. Purgathofer, "Combined rendering of polarization and fluorescence effects," *Proc. Eurographics Workshop on Rendering*, pp. 197-204, 2001.

[32] S. Guy and C. Soler, "Graphics gems revisited: fast and physically-based rendering of gemstones," *Proc. SIGGRAPH*, pp. 231-238, 2004.

[33] LightTools, `http://www.opticalres.com/`.

[34] ZEMAX, `http://www.zemax.com/`.

[35] OptiCAD, `http://www.opticad.com/`.

[36] W. H. Press, S. A. Teukolsky, W. T. Vetterling, and B. P. Flannery, *Numerical recipes in C: the art of scientific computing*, Cambridge University Press, 1992.

[37] K. Ikeuchi, "Reconstructing a depth map from intensity maps," *Proc. Int'l Conf. Pattern Recognition*, pp. 736-738, 1984.

[38] B. K. P. Horn, "Height and Gradient from Shading," *Int'l J. Computer Vision*, Vol. 5, No. 1, pp. 37-75, 1990.